Microtubule dynamics at the growth cone are mediated by α7 nicotinic receptor activation of a Gαq and IP_3 receptor pathway

Jacob C. Nordman and Nadine Kabbani[1]

Department of Molecular Neuroscience, Krasnow Institute for Advanced Study, George Mason University, Fairfax, Virginia, USA

ABSTRACT **The α7 nicotinic receptor (α7) plays an important role in neuronal growth and structural plasticity in the developing brain. We have recently characterized a G-protein-signaling pathway regulated by α7 that directs the growth of neurites in developing neural cells. Now we show that choline activation of α7 promotes a rise in intracellular calcium from local ER stores *via* Gαq signaling, leading to IP_3 receptor (IP_3R) activation at the growth cone of differentiating PC12 cells. A mutant α7 significantly attenuated in calcium conductance (D44A; $P<0.001$) was found to be unable to promote IP_3R signaling and calcium store release. In addition, calcium elevation *via* α7 correlates with a significant attenuation in the rate of microtubule invasion of the growth cone ($P<0.001$). This process was also attenuated in the D44A mutant and blocked by an inhibitor of the IP_3R, suggesting that calcium flow through the α7 channel and activation of the Gαq pathway are necessary for growth. Taken together, the findings reveal an inhibitory mechanism of α7 on cytoskeletal growth *via* the intracellular calcium activity of the receptor channel and the Gαq signaling pathway at the growth cone.—Nordman, J. C., Kabbani, N. Microtubule dynamics at the growth cone are mediated by α7 nicotinic receptor activation of a Gαq and IP_3 receptor pathway. *FASEB J.* 28, 2995–3006 (2014). www.fasebj.org**

Key Words: choline · heterotrimeric G protein · calcium stores · PIP_2 · EB3

Abbreviations: α7, α7 nicotinic acetylcholine receptor; Ab, antibody; ACh, acetylcholine; Bgtx, α-bungarotoxin; CICR, calcium-induced calcium release; DAG, diacyl glycerol; EB3, end-binding protein 3; ER, endoplasmic reticulum; F-actin, filamentous actin; fBgtx, fluorescein-conjugated α-bungarotoxin; Gαq, G-protein subunit αq; GAP-43, growth-associated protein 43; GC, growth cone; IgG, immunoglobulin G; IP_3, inositol triphosphate; IP_3R, inositol triphosphate receptor; KO, knockout; nAChR, nicotinic acetylcholine receptor; NGF, nerve growth factor; PC12, pheocromocytoma line 12; PH, pleckstrin homology; PIP_2, phosphatidylinositol-4,5-bisphosphate; RFP, red fluorescent protein; ROI, region of interest; Ry, ryanodine; RyR, ryanodine receptor; SA, surface area; SP, [D-Trp7,9,10]-substance P; WT, wild type; Xest C, xestospongin C

Acetylcholine (ACH) and its receptors play an important role in modulating neuronal growth and synapse formation in the brain (1, 2). Several nicotinic ACh receptors (nAChRs) are expressed early in nervous system development, thereby contributing to the formation of synaptic circuits (3). The α-bungarotoxin (Bgtx)-sensitive α7 nAChR (α7) is abundant in the developing brain and can play an important role in the maturation of axons and dendrites (1, 4). This receptor, which is localized to regions of cellular remodeling and growth, including axon growth cones (GCs) and dendritic spines (2, 4), has been shown to modulate cytoskeletal assembly (5). For example, in α7-knockout (KO; $\alpha7^{-/-}$) mice, newly born neurons of the dentate gyrus exhibit noticeable deficits in synaptic integration into CA3 due to deficits in dendritic branching (1). These developmental deficits may underlie memory and cognitive impairment observed in adult $\alpha7^{-/-}$ mice (6, 7).

On activation by ligands such as ACh, its membrane derivative choline, or the nAChR agonist nicotine, α7 channels conduct a sharp calcium current into the cell (8). In axons of hippocampal neurons, α7 activation has been linked to oscillatory increases in intracellular calcium underlying neurotransmitter release (9). This rise in intracellular calcium, which can persist for up to 30 min in brain slices and considerably less in cultured neurons (10, 11), is blocked by Bgtx and not detected in neurons of $\alpha7^{-/-}$ mice (9). Studies indicate that these persistent calcium fluctuations are driven by calcium flow through the α7 and downstream longer-lived changes in calcium-induced calcium release (CICR). This property of α7 appears to be dependent on the activation of inositol triphosphate receptors (IP_3Rs) in the endoplasmic reticulum (ER) (9).

In this study, we demonstrate a mechanism by which α7 mediates intracellular calcium release in growing neurites of differentiating neural cells. We show that

[1] Correspondence: Krasnow Institute for Advanced Study, 4400 University Dr., Fairfax, VA 22030, USA, E-mail: nkabbani@gmu.edu

doi: 10.1096/fj.14-251439

This article includes supplemental data. Please visit *http://www.fasebj.org* to obtain this information.

interaction with heterotrimeric G-protein subunit αq (Gαq) and activation of phosphatidylinositol-4,5-bisphosphate (PIP_2) enables α7-mediated CICR *via* IP_3Rs in the GC. This α7 pathway depends on calcium flow through the receptor channel and signaling through G proteins, thereby linking localized changes in calcium with the movement of the microtubule cytoskeleton.

MATERIALS AND METHODS

Cell culture

Pheocromocytoma line 12 (PC12) cell cultures were prepared as described previously (12), with minor modifications. In brief, 10-cm Petri dishes (Thermo Fisher Scientific, Waltham, MA, USA), 96 glass-bottom well culture plates (Life Technologies, Carlsbad, CA, USA), or 1.0 glass coverslips (Sigma, St. Louis, MO, USA) were precoated with poly-D-lysine (PDL; 100 μg/ml). PC12 cells were maintained in dMEM containing 10% horse serum, 5% FBS, and 1% penicillin-streptomycin (pen-strep) antibiotic (Life Technologies) at 37°C in a 5% CO_2-95% O_2 chamber. Cells were differentiated by the addition of 100 nM 2.5S nerve growth factor (NGF) at 3 d after plating or at 50% growth confluence (Life Technologies).

For transfections, mammalian expression vectors encoding the calcium sensor protein GCaMP5G (Addgene, Cambridge, MA, USA), the PIP_2 sensor PH-mCherry (Addgene), and the microtubule-capping protein end-binding protein 3–red fluorescent protein (EB3-RFP; Peter Baas, Drexel University, Philadelphia, PA, USA) were used as described previously (13–15). A mutant α7 (in pcDNA3.1) with a point mutation from aspartate to alanine at amino acid position 44 (D44A), which has been shown to significantly reduce calcium permeability of the channel, was used (16). Cells were transfected with Lipofectamine 2000 (Life Technologies) in serum-free medium for 6 h, 18 h after plating. Transfection medium was then replaced with dMEM containing NGF, as described above. Imaging experiments were performed 3 d after transfection. An empty pcDNA3.1 vector was used as a transfection control.

Drug treatment

Drug concentrations were determined on the basis of published studies and assessed in pilot experiments for effects on cell health using trypan blue (EMD, Darmstadt, Germany). For α7 activation, the selective receptor agonist choline (0.1–10 mM) was used (17). dMEM (11965-092; Life Technologies) is supplemented with 30 μM choline by the manufacturer, which has been shown necessary to maintain cell health and promote cell growth by contributing to stabilization of the plasma membrane. This concentration of choline, however, is presumed insufficient to activate α7, which is activated by much higher levels of choline (EC_{50} 1.6 mM; ref. 18). Intracellular calcium release, IP_3Rs, ryanodine receptors (RyRs), and Gαq were all inhibited by treating PC12 cells with thapsigargin (1 μM; Sigma), xestospongin C (Xest C; 1 μM; Tocris, Bristol, UK), ryanodine (Ry; 30 μM; Tocris), and [D-Trp7,9,10]-substance P (SP; 1 μM; Tocris), for 30 min, respectively (14). Experiments were performed in triplicate, and the data presented represent average values.

Immunocytochemistry

Cells were fixed in 1× PEM (80 mM PES, 5 mM EGTA, and 1 mM $MgCl_2$, pH 6.8) containing 0.3% glutaraldehyde at room temperature for 30 min (19). Cells were permeabilized in 0.05% Triton-X 100 prior to glutaraldehyde quenching with 10 mg/ml sodium borohydride, then blocked in 10 mg/ml BSA and 10% goat serum (Life Technologies) prior to antibody (Ab) or ligand staining. Immunocytochemistry was performed by adding the following primary Abs (1 μg/ml) overnight at 4°C: α-tubulin (Sigma), Gαq (Abcam, Cambridge, UK), and pIP_3R (Abcam). The addition of the following secondary Abs (4 μg/ml) was performed at room temperature for 1 h: carbocyanine (Cy) 2, Dylight 488, Dylight 560, and Alexa Fluor 647 (Jackson ImmunoResearch, West Grove, PA, USA). α7s were visualized using Alexa Fluor 647 fluorescein-conjugated Bgtx (fBgtx; Life Technologies). Filamentous actin (F-actin) was visualized using rhodamine phalloidin (Cytoskeleton, Denver, CO, USA). Fluorescence imaging was performed using a Nikon Eclipse 80i confocal microscope fitted with a Nikon C1 charge-coupled device camera (Nikon, Tokyo, Japan). Green, red, and deep red signals were visualized using 488-, 555-, and 641-nm excitation lasers, respectively. Images were captured using the EZ-C1 software (Nikon, Tokyo, Japan) and processed in ImageJ [U.S. National Institutes of Health (NIH), Bethesda, MD, USA].

Protein analysis

PC12 cell lysates were obtained by solubilizing proteins with a nondenaturing lysis buffer solution (1% Triton X-100, 137 mM NaCl, 2 mM EDTA, and 20 mM Tris HCl, pH 8) supplemented with protease and phosphatase inhibitors (Roche, Penzberg, Germany) at 4°C for 1 h. This solution has been shown to be effective in isolating α7s and their interactors from the plasma membrane (12). Isolation or immunoprecipitation of protein complexes from cells was conducted as described previously (20). In brief, 500 μg of cell lysate was layered over streptavidin-coated or protein G Dynabeads (Life Technologies) conjugated to biotin-α-Bgtx (Life Technologies), anti-Gαq polyclonal Abs (Abcam), or purified immunoglobulin G (IgG) Ab (Cell Signaling, Danvers, MA, USA) as an immunopreciptation control. Protein complexes were separated by gel electrophoresis on a 4–12% Bis-Tris gradient gel (Invitrogen) for Western blot analysis using the following Abs at 1 μg/ml: mAb 306 (21); Gαq, growth-associated protein 43 (GAP-43), IP_3R, and pIP_3R (Abcam); and GAPDH (Cell Signaling). Species-specific peroxidase-conjugated secondary Abs (Jackson ImmunoResearch) were used at a concentration of 0.4 μg/ml. Signals were detected using a SuperSignal West Pico Chemiluminescent Substrate (Thermo Fisher Scientific). SeeBlue and MagicMark (Life Technologies) were used as molecular weight standards. Blots were imaged using a Gel Doc imaging system (Bio-Rad, Hercules, CA, USA). Band density analysis was performed using ImageJ (NIH). All Western blot values are based on averages from 3 separate experiments.

Cellular calcium imaging

We used GCaMP5G for the visualization of rapid calcium fluctuations in PC12 cells (13). Imaging experiments were performed 3 d after transfection with GCaMP5G and/or a second vector. For drug treatment, cells were incubated with Xest C, SP, or BAPTA (30 μM) for 30 min prior to imaging. All imaging experiments were performed in an HBSS solution supplemented with 10 mM HEPES and warmed to 37°C. Calcium transients and dynamics were detected at an acquisition rate of 1 frame every 70 ms for 2 min at 2 × 2 binning on a Zeiss Axio Observer Z.1 with an attached mRM camera (Carl Zeiss, Oberkochen, Germany). Phototoxicity and pho-

tobleaching were minimized using neutral density and low-wavelength light filters as reported previously (4). Choline (0.1–10 mM) or choline and Bgtx (50 nM) prepared in HBSS were applied to the recording chamber at a flow rate of 1 ml/s *via* a gravity-fed perfusion system after 5 s (70 frames) of a baseline recording. HBSS alone was used as the vehicle control. Regions of interest (ROIs) were analyzed using ImageJ (NIH) and normalized as $\Delta F/F_0$. ROIs were averaged over conditions. The data presented have been normalized to HBSS controls. Ten cells were imaged per condition, all experiments were performed in triplicate, and the data presented represent average values (n=10).

Analysis of PIP_2 activation

PH-mCherry is a genetically encoded sensor for PIP_2 breakdown, allowing for the visualization of the phospholipase C pleckstrin homology (PH) domain translocation from the cell surface into the cytosol (14). We used an established protocol to examine PIP_2 activity *via* PH-mCherry (14). At 3 d after transfection with PH-mCherry (and the indicated GCaMP5G and/or D44A constructs), cells were washed with HBSS or preincubated with SP or BAPTA prior to imaging. PH-mCherry (excitation at 555 nm) was visualized at an acquisition rate of 1 frame every 5 s for 4 min at 2 × 2 binning. Drugs were applied after 20 s (4 frames) of a baseline recording. PH-mCherry translocation was determined by ROI analysis, measuring the fluorescence signal at within 1 μm of the edge of the cell (*i.e.*, the plasma membrane) and in the cytoplasm. Fluorescent values were normalized to area (μm^2) and measured using ImageJ (NIH). Translocation values were determined using the equation $(F_m - F_c)/(F_m + F_c)$, where F_m and F_c refer to PH-mCherry fluorescence at the (plasma) membrane and in the cytoplasm, respectively. Experiments were performed in triplicate, and the data presented are group averages. Five cells were imaged per condition, all experiments were performed in triplicate, and the data presented represent average values (n=5).

Microtubule motility assay using EB3-RFP comet analysis

EB3 is a microtubule-capping protein that binds to the free plus growing end of microtubules during active assembly (22). Fluorescently tagged EB3 proteins (EB3 comets) have been used to study the rate and directionality of neurite growth in PC12, as well as primary neurons (15, 23). We examined EB3 movement in PC12 cells 3 d after transfection with EB3-RFP (and GCaMP5G and/or D44A vectors). Imaging experiments were performed in an HBSS solution warmed to 37°C. For drug treatment, cells were preincubated with Xest C or a vehicle (0.1% DMSO) for 30 min prior to imaging. EB3 comet velocity was visualized in the GCs at an acquisition rate of 1 frame/s for 2 min at 2 × 2 binning (24). A baseline for EB3 motility was established for each recording for 5 s (5 frames) of acquisition. Comet trajectories were traced using ImageJ software (NIH). Five cells were imaged per condition, all experiments were performed in triplicate, and the data presented represent average values (n=5).

Neurite growth and statistical analysis

Reconstruction of neurites was performed using Neuromantic (25). Tubulin- and phalloidin-positive cells were assessed for NGF-induced changes in neurite surface area (SA). Only neurites longer than the soma were analyzed. Twenty to 30 cells were reconstructed from each group and then repeated in triplicate for group averages.

Statistical values were obtained using a 2-tailed Student's t test or 1-way ANOVA. Values of $P < 0.05$ were considered significant. All experiments were performed in triplicate, and group averages (means±SEM) are presented.

RESULTS

Neurite maturation is associated with enhanced α7 expression and calcium signaling

Recently we have shown a central role for α7 in the maturation of axons and neurites in PC12 cells, cortical neurons, and hippocampal neurons (4, 12). We examined expression and activity of endogenous α7s in differentiating PC12 cells. A quantitative analysis of the fBgtx signal in permeabilized cells was used to detect cellular α7s. Experiments indicate that during NGF differentiation, α7s are localized to sites of neurite branching and growth, most noticeably, GC. The α7 subunit was found in regions of cytoskeletal arrangement, which also stained for F-actin (phalloidin) and anti-tubulin Abs (**Fig. 1*A***). Nonlabeled Bgtx displaced the fBgtx signal in cells in a concentration-dependent manner, thus confirming the specificity of this fluorescent ligand for α7s (ref. 13 and data not shown).

PC12 cells were differentiated with 100 nM NGF and analyzed for α7 expression at various stages of maturation. After 3 d of treatment, NGF is known to have its strongest effect on PC12 cells, characterized by rapid neurite outgrowth, elaborate neurite fields, and complex branching (26). As shown in Fig. 1*B*, α7 subunit expression increases during NGF differentiation and correlates with a rise in the expression of the neurite growth regulatory protein GAP-43. This finding is corroborated by observations on elevation in α7 levels in the GCs during NGF differentiation (Fig. 1*A*) and suggests that α7 regulates neurite maturation and structure.

Calcium signaling through α7 has been shown to play an important role in the formation of synapses in the central nervous system (2). We examined cellular calcium changes *via* α7 at 3 d of NGF differentiation using the genetically encoded calcium sensor protein GCaMP5G (13). As shown in Fig. 1*C*, a strong calcium response was seen at the soma (224±46%), GC (813±78%), and in the growing neurite (487±67%) following α7 activation with the selective agonist choline (17). At the current imaging acquisition rate (70 ms/frame), however, the dynamics of calcium influx through the rapidly activating and deactivating α7 channel are not measurable. Choline-induced calcium rises in the neurite appeared later than in the GC, suggestive of back-propagation into the neurite from the GC. Choline-induced calcium occurred in a dose-dependent manner and was abolished by preapplication with Bgtx (Fig. 1*C*), confirming the specificity of choline on the α7. In nondifferentiated cells, choline did not produce a rise in cellular calcium (Fig. 1*C*), consis-

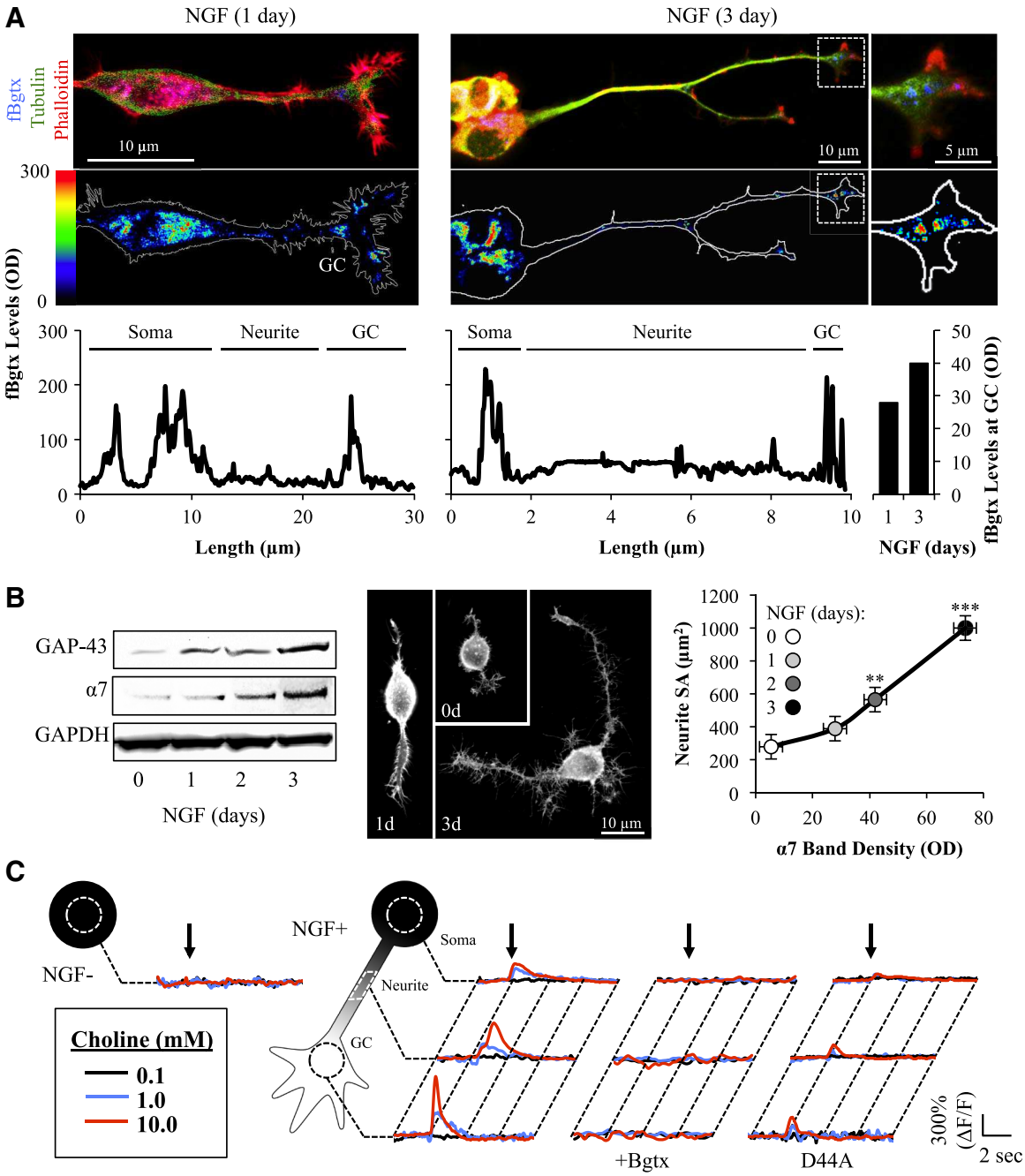

Figure 1. Up-regulation of α7s in differentiated PC12 cells. *A*) Detection of α7 subunits in 1 and 3 d NGF differentiated PC12 cells using fBgtx (blue), rhodamine phalloidin (red), and α-tubulin (green). Heat map shows the distribution of fBgtx in the cell. *B*) Left panel: Western blot detection of α7 and GAP-43 proteins during differentiation. GAPDH was used as a control. Middle panel: images of phalloidin-stained cells differentiated for 0, 1, and 3 d with NGF. Right panel: elevation in α7 levels during NGF differentiation and neurite growth (SA, surface area). *C*) α7-mediated calcium rises in the soma, neurite, and GC in response to choline. The GCaMP5G signal remained at baseline prior to differentiation (−NGF), or in differentiated cells preincubated with Bgtx for 1 min prior to imaging. Attenuated calcium responses were visualized in cells transfected with D44A. Arrow indicates time of drug application. Error bars indicate means ± SEM. $^{**}P < 0.01$, $^{***}P < 0.001$; Student's *t* test.

tent with the earlier finding that α7 expression is greatest during differentiation.

Site-specific mutations in the calcium-conducting pore of the α7 channel have enabled characterization of channel conductance under various conditions (27–29). A new mutant of the α7 (D44A; ref. 16) was used to examine the role of calcium flow in growth. PC12 cells transfected with D44A presented a lowered calcium response (−67±11%) compared to controls following choline treatment (Fig. 1*C*). In these experiments, an empty pcDNA3.1 vector was used as a transfection control. Consistent with findings on D44A function in hippocampal neurons (16), our calcium imaging data suggest that expression of this mutant

significantly diminishes calcium flow through the α7. A confirmation of D44A expression in PC12 cells indicates that expression of D44A increases total fBgtx fluorescence (by 89±15%) without altering the overall cellular distribution of the signal (Supplemental Fig. S1). The data are strongly suggestive that D44A is integrated into functional α7s in the cell, but because neither fBgtx nor the anti-α7 Ab distinguishes between D44A and the endogenous α7 subunit, it is not possible to quantify the amount of D44A in these cells.

α7 activation promotes IP_3R calcium release from internal stores

Recent studies have shown that presynaptic α7s promote calcium release from intracellular stores *via* IP_3Rs, thereby regulating glutamate release at hippocampal synapses (9). We postulate that α7-mediated store release can contribute to the maturation of the neurite. We assessed the distribution of IP_3Rs at the GC in differentiated PC12 cells. As shown in **Fig. 2*A***, IP_3Rs were most prominent at the central zone. A strong colocalization of the signal for the ER-Tracker Red with fBgtx or with the IP_3R Ab (Fig. 2*A* and Supplemental Fig. S2) suggests that α7s are in proximity to calcium stores at the GC.

We tested the involvement of IP_3Rs and RyRs in choline-associated calcium elevation at the GC. To determine the contribution of α7, cells were preincubated with the IP_3R selective blocker Xest C (1 μM) and Ry, which at high concentrations (30 μM), fully blocks the RyR. As shown in Fig. 2*B*, preincubation with Xest C almost completely abolished the α7 calcium signal at the GC at the measured time scale of 1 frame every 100 ms. In contrast, Ry had little effect on choline-mediated calcium responses. The effect of Xest C was commensurate with that of thapsigargin (Fig. 2*B*), a nonspecific intracellular store inhibitor, suggesting that α7s mediate calcium release by regulating IP_3Rs in the ER of the GC.

Within GCs, spontaneous transient elevations of intracellular calcium have been shown to critically regulate neurite growth (30). In spinal cord neurons, these transient calcium signals have been found to inhibit neurite extension (30). We examined α7-induced calcium elevations in the GC and the growing neurite. A multipoint tracking method was used to measure changes in the GCaMP5G signal along the neurite and in ER-containing domains identified by ER Tracker Red (Fig. 2*C*). As shown in Fig. 2*C*, ROI analysis revealed α7-induced calcium elevations that start at the GC (~0.5 s after drug application) and then back-propagate into the neurite. Correlation analysis revealed that calcium levels were strongest in ER domains of the neurite (slope=8.9%; Fig. 2*D*). Preincubation with Xest C abolished the calcium rise in the GC, and little diffusion was observed in the neurite (slope=0.1%; Fig. 2*C*, *D*). The expression of D44A was also found to attenuate the calcium signal in the GC (Fig. 2*C*, *D*; slope=2.8%), thus supporting the hypothesis that calcium flow through α7 is necessary for CICR from the ER in the neurite. To confirm this, we examined α7-mediated calcium changes under calcium-buffering conditions using BAPTA. In the presence of BAPTA, choline (0.1–10 mM) did not promote a rise in calcium within the cell (Supplemental Fig. S3).

Coupling to Gαq enables α7-mediated CICR at the GC

Canonical Gαq signaling can directly regulate the levels of calcium in the GC *via* the generation of IP_3 (31). Recently, we have shown that interaction between α7 and G proteins modulates neuronal growth (4, 32, 33). To test interactions between α7 and Gαq, α7 interactomes from 3 d differentiated PC12 cells were isolated using a biotin-conjugated Bgtx pulldown assay. Western blot detection of Gαq proteins within the pulldown experiment revealed association between the receptor and the G-protein subunit (**Fig. 3*A***). An experiment in which an anti-Gαq Ab was used to coimmunoprecipitate the α7 subunit confirmed association between α7 and Gαq in PC12 cells. HCN1 was used as a negative control in the interaction assay (Fig. 3*A*). Immunofluorescence detection of endogenous Gαq and α7 using an anti-Gαq Ab and fBgtx, respectively, demonstrated coexpression of the two proteins in the central zone of the GC (Fig. 3*B*).

Calcium imaging was performed to test the contribution of Gαq activity on α7-mediated calcium signaling in the GC. Experiments conducted in cells preincubated with the selective Gαq inhibitor SP (34) indicate that choline-mediated elevation in calcium is largely abolished in the presence of SP (Fig. 3*C*). Indeed, even at the highest choline concentration tested (10 mM), SP was able to block the calcium signal in the GC, suggesting that Gαq activity is necessary and downstream of the α7. In these experiments, SP did not cause a change in KCl-evoked calcium rise (Fig. 3*C*).

Choline-mediated phosphorylation of IP_3Rs at the GC depends on Gαq

In neurons, calcium flow from IP_3Rs into the cytosol plays an important role in axon growth and maturation (31). In turn, the gating of the IP_3R is determined by fluctuations in cytosolic calcium, including the activity of calcium-sensitive kinases and phosphatases (35–37). To examine whether interaction between α7s and Gαq affects IP_3Rs in the GC, we monitored a functional phosphorylation site in the IP_3R that has been shown to correlate with receptor opening (38). Using an Ab that recognizes the phosphorylated form of the IP_3R (pIP_3R) at serine residue 1598, a site for PKC phosphorylation (38), we tested the effect of choline on the IP_3R. As shown in **Fig. 4*A*, *B***, a 1 min treatment of choline led to a significant increase in pIP_3R levels in the cell. The strongest pIP_3R signal was observed in the GC (Fig.

4*B–D*). The effect of choline on IP_3R phosphorylation was concentration dependent and diminished by preincubation with Bgtx (Fig. 4*A*). We tested the role of Gαq in IP_3R phosphorylation. Preincubation with SP blocked the effect of choline on phosphorylation of the IP_3R (Fig. 4). Similarly, expression of the D44A subunit mutant was also found to attenuate the effect of choline on pIP_3R levels (Fig. 4), suggesting that calcium flow through the α7 channel and activation of Gαq can contribute to IP_3R function in the cell.

α7/Gαq signaling promotes PIP_2 breakdown

Gαq regulates IP_3R-mediated calcium release from the ER by promoting the breakdown of PIP_2 into IP_3 and diacyl glycerol (DAG) (36, 39). The breakdown of PIP_2 by phospholipase C is associated with dynamic movement of the phospholipid from the plasma membrane into the cytoplasm. This process can be measured in real time using the genetically encoded sensor PH-mCherry (14). We tested the effect of α7 on PIP_2

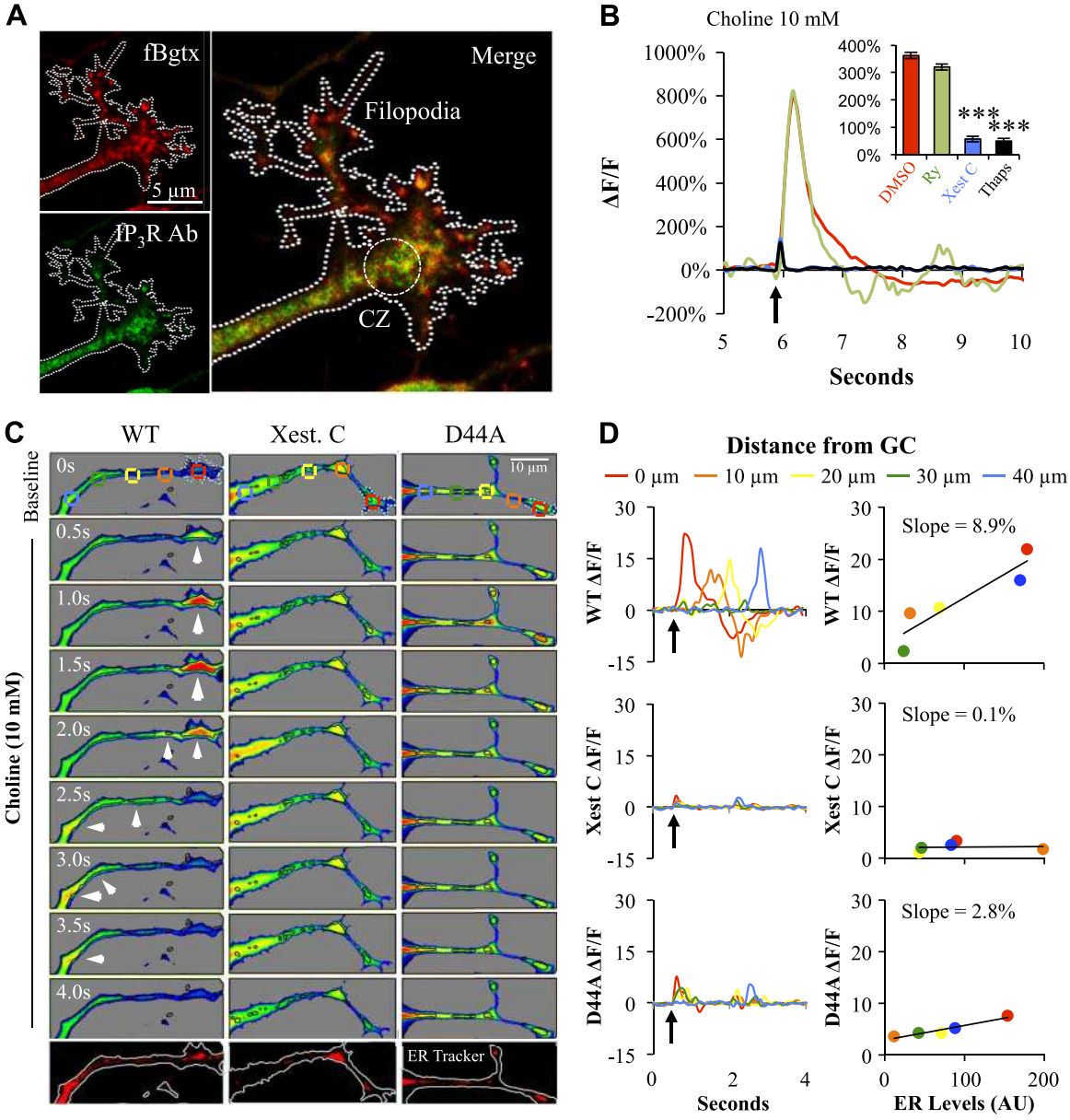

Figure 2. α7 promotes IP_3R-mediated calcium release at the GC. *A*) Colocalization of fBgtx and anti-IP_3R Ab staining in the central zone (CZ) of the GC. *B*) α7-mediated calcium signaling in the GC is abolished in the presence of 1 μM thapsigargin (Thaps) or Xest C, but not 30 μM Ry. DMSO was used as a vehicle control. *C*) α7-mediated calcium elevation in the GC and proximal neurite. Live imaging of GCaMP5G and ER-Tracker Red in cells treated with 10 mM choline (beginning at 0.5 s). Images: WT (left panels); preincubated with Xest C (middle panels); transfected with D44A (right panels). Boxed areas in top panels represent ROIs of the GCaMP5G signal, shown as a heat map at the GC (0 μm) and 10–40 μm into the neurite. ER is outlined in black. Bottom panels: ER-Tracker labeling in the neurite. *D*) Average values from *C* showing changes in calcium (left panels) and a correlation of peak calcium rises relative to the detection of the ER-Tracker signal in the GC and adjoining neurite (right panels). Error bars = means ± SEM. ***$P < 0.001$; Student's *t* test.

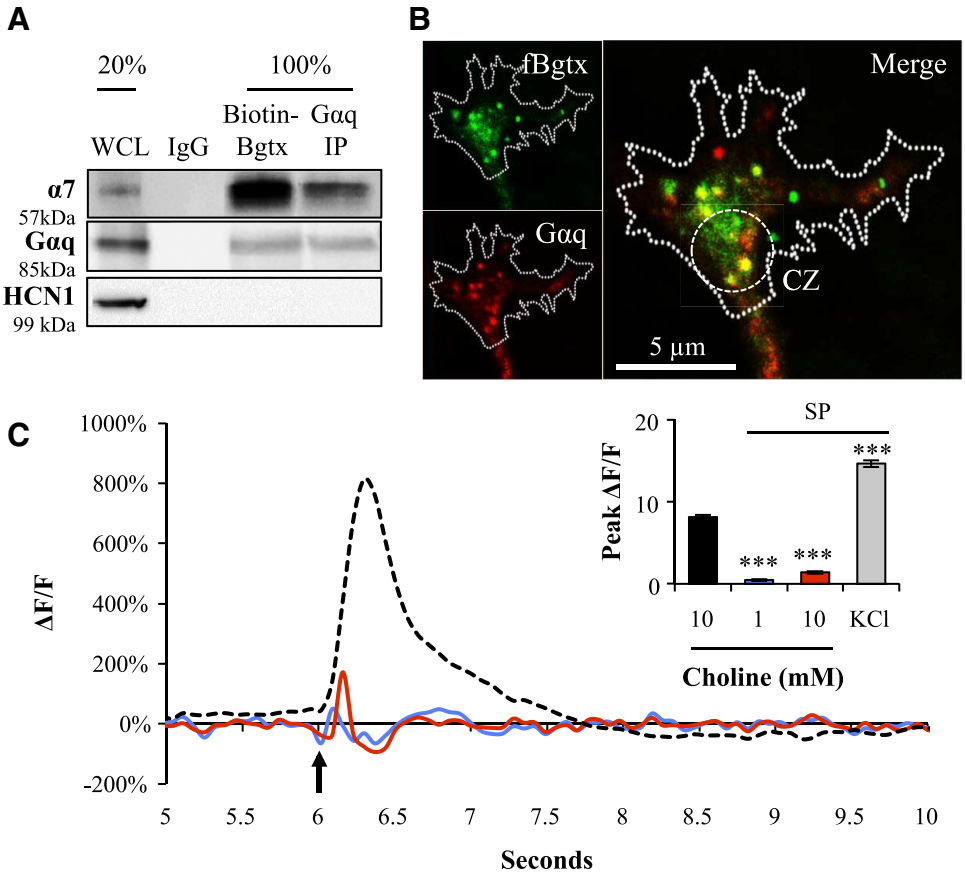

Figure 3. α7 calcium release at the GC is mediated by association with Gαq. *A*) Western blot detection of α7 and Gαq interactions from differentiating PC12 cells. Biotin-conjugated Bgtx and anti-Gαq Abs were used to isolate α7 and Gαq protein complexes, respectively. Anti-HCN1 Ab was used as negative control. Twenty percent of whole cell lysate (WCL) was used relative to protein for pulldown and immunoprecipitation; 100% was used to detect total levels in the cell. IgG Ab was used as an immunoprecipitation control and was used in equal amounts to the anti-Gαq Ab. *B*) Immunofluorescent detection and colocalization of α7 and Gαq in the CZ of the GC. *C*) α7 calcium signaling in the GC in response to 1 and 10 mM choline application or KCl (50 mM) and in the presence of the Gαq inhibitor SP (1 μM). Arrow indicates the time of drug application. Error bars = means ± SEM. $^{***}P < 0.001$; Student's *t* test.

breakdown and translocation in the GC. PC12 cells were cotransfected with PH-mCherry and GCaMP5G, enabling simultaneous detection of PIP_2 and calcium changes. Activation of the muscarinic ACh receptor by carbachol (CCh) was used to confirm PH-mCherry detection of PIP_2 breakdown (ref. 14 and **Fig. 5**). Choline treatment (10 mM) was also associated with a translocation of PH-mCherry from the cell surface to the cytosol in the neurite and GC concurrent with its effect on the calcium rise (Fig. 5). The strongest effect of choline on PH-mCherry translocation and GCaMP5G fluorescence was observed in the GC (Fig. 5).

To ensure involvement of Gαq in α7-mediated PIP_2 breakdown, cells cotransfected with PH-mCherry and GCaMP5G were preincubated with SP prior to imaging. As shown in Fig. 5, SP abolished choline-induced translocation of PH-mCherry, as well as GCaMP5G signaling in the neurite and GC. Taken together, the data suggest that α7-mediated calcium promotes breakdown of PIP_2 locally within the GC *via* Gαq. This finding is consistent with choline's effects on IP_3R activation (Fig. 4), supporting a mechanism of α7-mediated generation of IP_3 *via* PIP_2.

An α7/Gαq/IP_3R calcium mechanism underlying inhibition of microtubule growth

The initiation, growth, and guidance of axons require the regulation of cytoskeletal proteins (31). Actin filament polymerization is essential for membrane protrusion underlying neurite guidance, but the overall development and branching of the axon require the assembly of microtubules and their entry into filopodia (40). We assessed the effect of α7 signaling on microtubule invasion of GC filopodia. Cells were cotransfected with GCaMP5G and the microtubule-capping protein, EB3 conjugated to RFP (EB3-RFP), which enabled us to measure calcium and cytoskeletal changes in real time in the GC. This EB3 capping protein is capable of tracking dynamic changes at the plus end of the microtubule structure and thus serves as a tool of analysis for neurite growth (4, 15). EB3-RFP proteins were detected throughout the GC (**Fig. 6*A***). In particular, a strong EB3-RFP signal was seen in the central zone, a region rich in microtubule invasion (41) and α7/Gαq/IP_3R expression. We examined the velocity of the EB3-RFP comets that invade filopodia at various concentrations of choline (0.1–10 mM). As shown in Fig. 6*A–C*, under basal conditions, EB3-RFP velocity was measured at 150 nm/s. After 2 min of choline treatment (1 mM), EB3-RFP velocity was reduced to 10 nm/s (Fig. 6*A–C*). At higher choline concentrations (10 mM) EB3-RFP movement reversed directions from anterograde to retrograde (−60 nm/s; Fig. 6*A*), consistent with GC collapse (Fig. 6*B, C* and refs. 4, 42). In fact, retrogradely moving EB3-RFP comets after choline application (1–10 mM) appeared to promote a collapse of the GC within 8 min of analysis (Fig. 6*B*). Calcium imaging at the same ROI indicates that the dose-dependent peaks in intracellular calcium

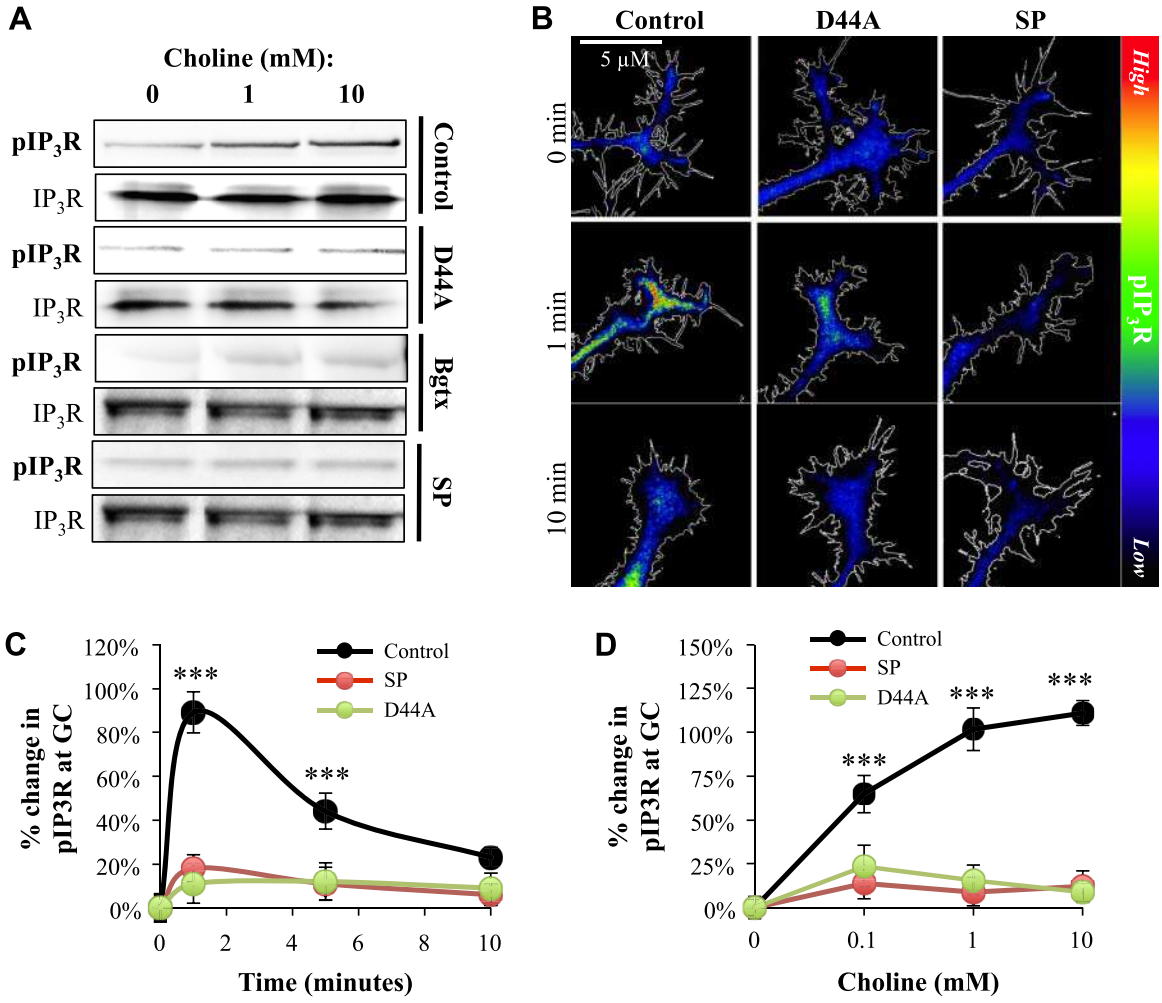

Figure 4. α7 activation promotes IP_3R phosphorylation *via* Gαq. *A*) Detection of the IP_3R and pIP_3R following a 1 min choline (0–10 mM) treatment in PC12 cells (control) and PC12 cells transfected with D44A, preincuabed with 50 nM Bgtx (1 min), or 1 μM SP (30 min). *B*) Cells were transfected with an empty pcDNA3.1 vector (control) or D44A. An anti-pIP_3R Ab was used to visualize pIP_3R expression at 0, 1, and 10 min choline treatment (10 mM). Cells were preincubated with SP 30 min prior to choline treatment. *C, D*) Average values for the percentage change in pIP_3R immunofluorescence from baseline (0 min in *C*; 0 mM choline in *D*) in the GC. Error bars = means ± SEM. ***$P < 0.001$; Student's *t* test.

in the GC achieved by 0.1–10 mM choline correlates with the overall reduction in EB3-RFP velocity when averaged over 2 min (Fig. 6*B, C*). The findings corroborate earlier data on the effect of α7 calcium signaling on microtubule growth, and are underscored by the finding that effects of choline on EB3-RFP velocity and GCaMP5G fluorescence are entirely abolished by preapplication of Bgtx (Supplemental Fig. S4).

To examine the involvement of IP_3Rs in α7-mediated regulation of cytoskeletal movement in the GC, cells were preincubated with Xest C 30 min prior to analysis. Xest C rendered a strong inhibitory effect on choline modulation of EB3-RFP velocity and GCaMP5G signaling, thereby restoring EB3-RFP movement to anterograde (Fig. 6*A, D*). Xest C, however, did have ancillary effects on EB3-RFP velocity, reducing microtubule movement by ~50%. The mutant D44A was also tested in the assay, and as shown in Fig. 6*A, C*, expression of D44A significantly attenuated the effects of choline on EB3-RFP velocity and directionality, consistent with its diminished effect on calcium in the GC. Taken together, the findings confirm the role of α7 calcium signaling in mobilization of calcium store release from IP3Rs at the GC and suggest that this mechanism regulates neurite growth.

DISCUSSION

Metabotropic functions of α7 are driven by calcium flow through the channel

nAChRs belong to a class of cys-loop ligand-gated receptors, which modulate neuronal activity by conducting ions across the plasma membrane (43). A number of cys-loop receptors, including the glycine channel, can directly bind G proteins *via* conserved motifs within their intracellular M3-M4 loop (44). Evidence now suggests that in addition to being regulated by G proteins, cys-loop receptors, including

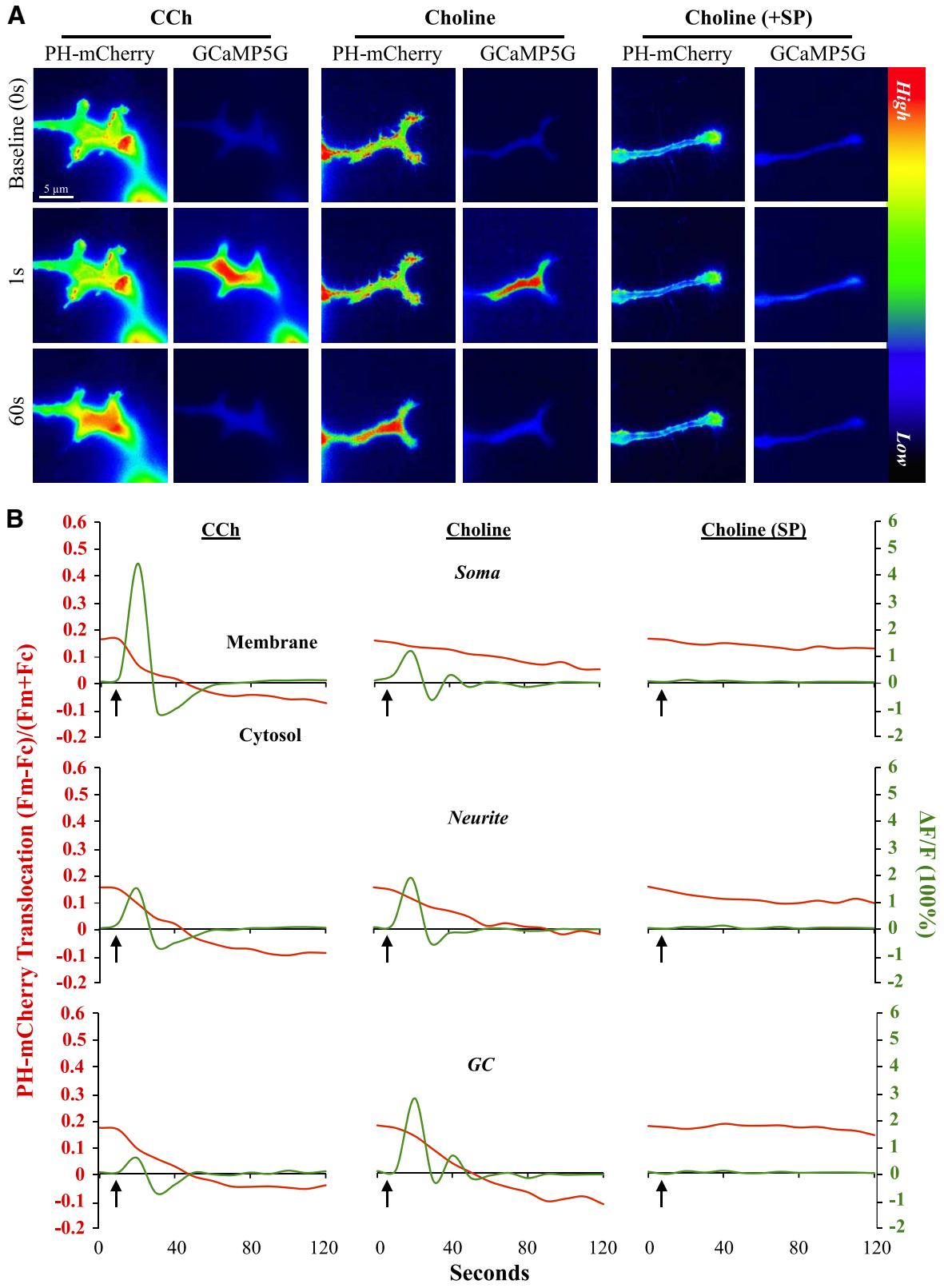

Figure 5. α7 promotes PIP_2 breakdown in the GC. PC12 cells were cotransfected with PH-mCherry and GCaMP5G 24 h prior to imaging. *A*) Representative images of PH-mCherry and GCaMP5G at the GC in cells treated with carbachol (CCh; 100 μM), choline (10 mM), or choline and SP (1 μM). *B*) Detection of PH-mCherry (red) and GCaMP5G (green) in the soma, neurite, and GC from cells treated with CCh or choline with or without SP preincubation. A measure of PH-mCherry translocation is described in Materials and Methods.

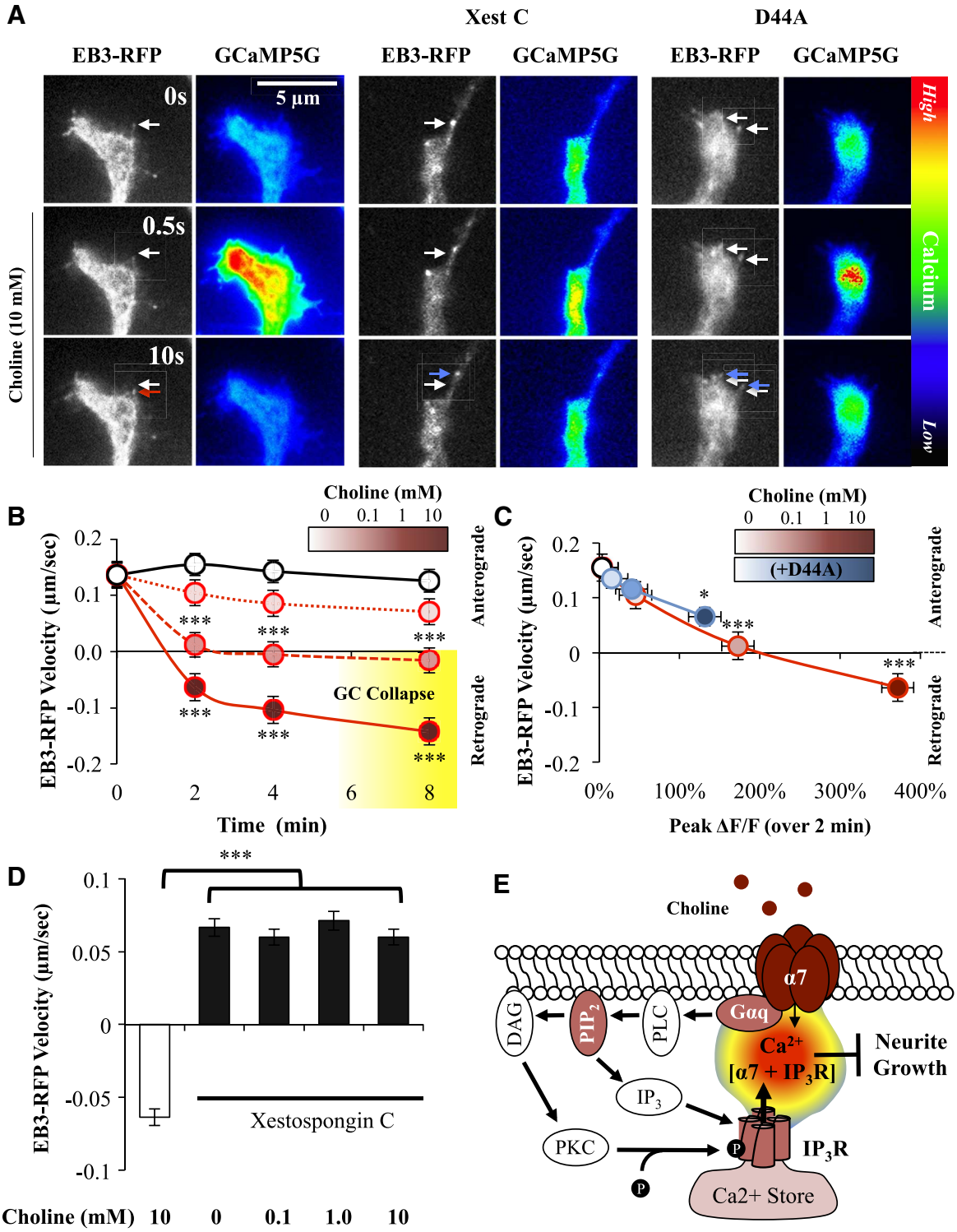

Figure 6. α7 calcium signaling inhibits microtubule growth *via* the IP_3R. *A*) Time-lapse imaging of EB3-RFP and GCaMP5G in the GC. Xest C, cells preincubated with Xest C 30 min prior to analysis; D44A, cells transfected with D44A. Beginning time point (white arrow) and end time point [red (backward) or blue (forward) arrow] indicated. *B*) Time course of choline-mediated changes in EB3-RFP velocity. Period of GC collapse is indicated in yellow. *C*) Correlation of the GCaMP5G signal peak and EB3-RFP comet velocity during choline treatment (averaged during 2 min of cell imaging). Control, no choline added; D44A, cells transfected with D44A. *D*) Cells were preincubated with Xest C for 30 min prior to choline treatment. *E*) Model showing a mechanism of α7/Gαq coupling underlying IP_3R calcium store release at the GC during neurite growth. Tested components of the pathway are shown in red. Error bars = SEM. $^*P < 0.05$, $^{***}P < 0.001$; Student's *t* test.

nAChRs, can also contribute to metabotropic signaling and second messenger production in the cell (33). We have recently shown that α7 regulates neuronal signaling and growth through Gαi/o in hippocampal neurons (4, 12, 33). A similar nAChR signaling mechanism exists in T cells, where α4 nAChRs can couple to Gαi/o and regulate cytokine release (45). Direct coupling to G proteins is of particular significance to nAChR activity in immune cells, where no nAChR current has been detected to date. Because studies reveal that several nAChRs, including α4β2 and α3β4α5, interact with Gα and βγ subunits (46, 47), it is increasingly accepted that nAChRs maintain ionotropic and metabotropic properties in cells.

The utility of the recently characterized D44A receptor mutant, which is significantly impaired in calcium conductance due to a mutation in the calcium pore, has enabled us to examine the involvement of calcium flow through the channel in signaling and neurite growth. Our findings indicate that calcium flow through the α7 is necessary for downstream regulation of IP_3Rs, as well as CICR from the ER in the growing neurite. The involvement of other receptors or channels as a downstream consequence of α7 activation cannot be completely ruled out at this point. Expression of D44A, which did not appear to alter the distribution of α7 in the cell, did, however, abolish the effect of choline on microtubule movement, suggesting that α7 function is contingent on the ability of the channel to conduct calcium. In light of this, our data suggest that the intracellular signaling and metabotropic properties of the α7 are intimately paired to its ionotropic activity.

α7 regulates calcium store release at the GC and modulates microtubule growth

The localization, concentration, and temporal aspects of the cellular calcium signal play a complex role in regulating neurite growth and synaptic development. In neurons, high levels of intracellular calcium can shift the cell into an antigrowth state, marked by a dramatic decrease in neurite growth paralleled by an attenuation of cytoskelelal elongation (31, 48). We find that choline, at a concentration adequate to fully activate α7, can foster high calcium levels within the GC *via* its actions on channel opening and CICR from the ER in PC12 cells. Similar mechanisms are predicted to exist in neurons of the nervous system, where the same signaling pathway may contribute to presynaptic growth and possibly neurotransmitter release. Interaction with Gαq and subsequent downstream signaling *via* PIP_2 appears central to the effect of α7 on calcium-driven shunting of neurite growth, marked by a slowing of microtubule invasion into filopodia and a reversal in directionality. Furthermore, at high levels of calcium, α7 activity leads to a collapse of the GC, possibly due to the activity of calcium sensitive proteases, such as calpain (49). This is supported by our observation that calcium elevations and EB3 protein movement are most affected in neurite regions that contain both α7 and the ER protein marker. These findings are consistent with earlier observations on the effect of α7 on overall decline in axonal growth and structural branching in hippocampal neurons (4) and suggest the involvement of Gαq-mediated calcium store release in this process.

The targeting and function of the α7 at the GC appear to be driven by interaction with scaffold proteins such as G protein-regulated inducer of neurite outgrowth 1 (Gprin1; ref. 12). Interestingly, Gprin1 can also regulate the trafficking and activity of Gαo at the GC (50), suggesting a role for this scaffold in α7/G protein interaction. Our experiments indicate that the targeting of α7 to the GC during cellular differentiation is necessary for calcium signaling and modulation of neurite growth. The coordinated responses of various G proteins to α7 activation thus appear to be critical in this process. FJ

The authors thank Dr. Jerrel Yakel and Ms. Pattie Lamb (National Institute of Environmental Health Science, Research Triangle Park, NC, USA) for receptor constructs. The authors also thank Justin King for technical assistance. This work is supported by a Wings for Life Spinal Cord Research grant award.

REFERENCES

1. Campbell, N. R., Fernandes, C. C., Halff, A. W., and Berg, D. K. (2010) Endogenous signaling through α7-containing nicotinic receptors promotes maturation and integration of adult-born neurons in the hippocampus. *J. Neurosci.* **30,** 8734–8744
2. Lozada, A. F., Wang, X., Gounko, N. V., Massey, K. A., Duan, J., Liu, Z., and Berg, D. K. (2012) Glutamatergic synapse formation is promoted by α7-containing nicotinic acetylcholine receptors. *J. Neurosci.* **32,** 7651–7661
3. Dwyer, J. B., Broide, R. S., and Leslie, F. M. (2008) Nicotine and brain development. *Birth Defects Res. C Embryo Today* **84,** 30–44
4. Nordman, J. C., Phills, W. S., Kodama, N., Clark, S. G., Del Negro, C. A., and Kabbani, N. (2013) Axon targeting of the alpha 7 nicotinic receptor in developing hippocampal neurons by Gprin1 regulates growth. [E-pub ahead of print] *J. Neurochem.* doi: 10.1111/jnc.12641
5. Shoop, R. D., Yamada, N., and Berg, D. K. (2000) Cytoskeletal links of neuronal acetylcholine receptors containing α7 subunits. *J. Neurosci.* **20,** 4021–4029
6. Young, J. W., Meves, J. M., Tarantino, I. S., Caldwell, S., and Geyer, M. A. (2011) Delayed procedural learning in α7-nicotinic acetylcholine receptor knockout mice. *Genes Brain Behav.* **10,** 720–733
7. Fernandes, C., Hoyle, E., Dempster, E., Schalkwyk, L. C., and Collier, D. A. (2006) Performance deficit of α7 nicotinic receptor knockout mice in a delayed matching-to-place task suggests a mild impairment of working/episodic-like memory. *Genes Brain Behav.* **5,** 433–440
8. Berg, D. K., and Conroy, W. G. (2002) Nicotinic α7 receptors: synaptic options and downstream signaling in neurons. *J. Neurobiol.* **53,** 512–523
9. Zhong, C., Talmage, D. A., and Role, L. W. (2013) Nicotine elicits prolonged calcium signaling along ventral hippocampal axons. *PLoS One* **8,** e82719
10. Del Barrio, L., Egea, J., Leon, R., Romero, A., Ruiz, A., Montero, M., Alvarez, J., and Lopez, M. G. (2011) Calcium signalling mediated through α7 and non-α7 nAChR stimulation is differentially regulated in bovine chromaffin cells to induce catecholamine release. *Br. J. Pharmacol.* **162,** 94–110
11. Liu, Q., and Berg, D. K. (1999) Actin filaments and the opposing actions of CaM kinase II and calcineurin in regulating α7-containing nicotinic receptors on chick ciliary ganglion neurons. *J. Neurosci.* **19,** 10280–10288

12. Nordman, J. C., and Kabbani, N. (2012) An α7 nicotinic receptor-G protein pathway complex regulates neurite growth in neural cells. *J. Cell Sci.* **125,** 5502–5513
13. Akerboom, J., Chen, T. W., Wardill, T. J., Tian, L., Marvin, J. S., Mutlu, S., Calderon, N. C., Esposti, F., Borghuis, B. G., Sun, X. R., Gordus, A., Orger, M. B., Portugues, R., Engert, F., Macklin, J. J., Filosa, A., Aggarwal, A., Kerr, R. A., Takagi, R., Kracun, S., Shigetomi, E., Khakh, B. S., Baier, H., Lagnado, L., Wang, S. S., Bargmann, C. I., Kimmel, B. E., Jayaraman, V., Svoboda, K., Kim, D. S., Schreiter, E. R., and Looger, L. L. (2012) Optimization of a GCaMP calcium indicator for neural activity imaging. *J. Neurosci.* **32,** 13819–13840
14. Chisari, M., Saini, D. K., Cho, J. H., Kalyanaraman, V., and Gautam, N. (2009) G protein subunit dissociation and translocation regulate cellular response to receptor stimulation. *PLoS One* **4,** e7797
15. Liu, M., Nadar, V. C., Kozielski, F., Kozlowska, M., Yu, W., and Baas, P. W. (2010) Kinesin-12, a mitotic microtubule-associated motor protein, impacts axonal growth, navigation, and branching. *J. Neurosci.* **30,** 14896–14906
16. Colon-Saez, J. O., and Yakel, J. L. (2013) A mutation in the extracellular domain of the α7 nAChR reduces calcium permeability. [E-pub ahead of print] *Pflügers Arch.* doi: 10.1007/s00424-013–1385-y
17. Khiroug, S. S., Harkness, P. C., Lamb, P. W., Sudweeks, S. N., Khiroug, L., Millar, N. S., and Yakel, J. L. (2002) Rat nicotinic ACh receptor α7 and β2 subunits co-assemble to form functional heteromeric nicotinic receptor channels. *J. Physiol.* **540,** 425–434
18. Alkondon, M., Pereira, E. F., Cortes, W. S., Maelicke, A., and Albuquerque, E. X. (1997) Choline is a selective agonist of alpha7 nicotinic acetylcholine receptors in the rat brain neurons. *Eur. J. Neurosci.* **9,** 2734–2742
19. He, Y., Francis, F., Myers, K. A., Yu, W., Black, M. M., and Baas, P. W. (2005) Role of cytoplasmic dynein in the axonal transport of microtubules and neurofilaments. *J. Cell Biol.* **168,** 697–703
20. Kabbani, N. (2007) Intracellular complexes of the β2 subunit of the nicotinic acetylcholine receptor in brain identified by proteomics. *Proc. Natl. Acad. Sci. U.S.A.* **104,** 6
21. Lindstrom, J., Schoepfer, R., Conroy, W. G., and Whiting, P. (1990) Structural and functional heterogeneity of nicotinic receptors. *Ciba Found. Symp.* **152,** 23–42; discussion 43–52
22. Stepanova, T., Slemmer, J., Hoogenraad, C. C., Lansbergen, G., Dortland, B., De Zeeuw, C. I., Grosveld, F., van Cappellen, G., Akhmanova, A., and Galjart, N. (2003) Visualization of microtubule growth in cultured neurons via the use of EB3-GFP (end-binding protein 3-green fluorescent protein). *J. Neurosci.* **23,** 2655–2664
23. Kelly, T. A., Katagiri, Y., Vartanian, K. B., Kumar, P., Chen, I. I., Rosoff, W. J., Urbach, J. S., and Geller, H. M. (2010) Localized alteration of microtubule polymerization in response to guidance cues. *J. Neurosci. Res.* **88,** 3024–3033
24. Nadar, V. C., Ketschek, A., Myers, K. A., Gallo, G., and Baas, P. W. (2008) Kinesin-5 is essential for growth-cone turning. *Curr. Biol.* **18,** 1972–1977
25. Myatt, D. R., and Nasuto, S. J. (2008) Improved automatic midline tracing of neurites with Neuromantic. *BMC Neurosci.* **9**(Suppl. 1), P81
26. Gunning, P. W., Letourneau, P. C., Landreth, G. E., and Shooter, E. M. (1981) The action of nerve growth factor and dibutyryl adenosine cyclic 3′:5′-monophosphate on rat pheochromocytoma reveals distinct stages in the mechanisms underlying neurite outgrowth. *J. Neurosci.* **1,** 1085–1095
27. Placzek, A. N., Grassi, F., Meyer, E. M., and Papke, R. L. (2005) An α7 nicotinic acetylcholine receptor gain-of-function mutant that retains pharmacological fidelity. *Mol. Pharmacol.* **68,** 1863–1876
28. Colon-Saez, J. O., and Yakel, J. L. (2011) The α7 nicotinic acetylcholine receptor function in hippocampal neurons is regulated by the lid composition of the plasma membrane. *J. Physiol.* **589,** 3163–3174
29. Criado, M., Svobodova, L., Mulet, J., Sala, F., and Sala, S. (2011) Substitutions of amino acids in the pore domain of homomeric α7 nicotinic receptors for analogous residues present in heteromeric receptors modify gating, rectification, and binding properties. *J. Neurochem.* **119,** 40–49
30. Lautermilch, N. J., and Spitzer, N. C. (2000) Regulation of calcineurin by growth cone calcium waves controls neurite extension. *J. Neurosci.* **20,** 315–325
31. Henley, J., and Poo, M. M. (2004) Guiding neuronal growth cones using Ca^{2+} signals. *Trends Cell Biol.* **14,** 320–330
32. Nordman, J. C., and Kabbani, N. (2012) An interaction between α7 nicotinic receptors and a G-protein pathway complex regulates neurite growth in neural cells. *J. Cell Sci.* **125,** 5502–5513
33. Kabbani, N., Nordman, J. C., Corgiat, B. A., Veltri, D. P., Shehu, A., Seymour, V. A., and Adams, D. J. (2013) Are nicotinic acetylcholine receptors coupled to G proteins? *Bioessays* **35,** 1025–1034
34. Mukai, H., Munekata, E., and Higashijima, T. (1992) G protein antagonists. A novel hydrophobic peptide competes with receptor for G protein binding. *J. Biol. Chem.* **267,** 16237–16243
35. Krizanova, O., and Ondrias, K. (2003) The inositol 1,4,5-trisphosphate receptor–transcrtional regulation and modulation by phosphorylation. *Gen. Physiol. Biophys.* **22,** 295–311
36. Ferris, C. D., Huganir, R. L., Bredt, D. S., Cameron, A. M., and Snyder, S. H. (1991) Inositol trisphosphate receptor: phosphorylation by protein kinase C and calcium calmodulin-dependent protein kinases in reconstituted lid vesicles. *Proc. Natl. Acad. Sci. U.S.A.* **88,** 2232–2235
37. DeSouza, N., Reiken, S., Ondrias, K., Yang, Y. M., Matkovich, S., and Marks, A. R. (2002) Protein kinase A and two phosphatases are components of the inositol 1,4,5-trisphosphate receptor macromolecular signaling complex. *J. Biol. Chem.* **277,** 39397–39400
38. Vanderheyden, V., Devogelaere, B., Missiaen, L., De Smedt, H., Bultynck, G., and Parys, J. B. (2009) Regulation of inositol 1,4,5-trisphosphate-induced Ca^{2+} release by reversible phosphorylation and dephosphorylation. *Biochim. Biophys. Acta* **1793,** 959–970
39. Yamaguchi, Y., Shirai, Y., Matsubara, T., Sanse, K., Kuriyama, M., Oshiro, N., Yoshino, K., Yonezawa, K., Ono, Y., and Saito, N. (2006) Phosphorylation and up-regulation of diacylglycerol kinase gamma via its interaction with protein kinase Cγ. *J. Biol. Chem.* **281,** 31627–31637
40. Kalil, K., and Dent, E. W. (2013) Branch management: mechanisms of axon branching in the developing vertebrate CNS. *Nat. Rev. Neurosci.* **15,** 7–18
41. Dent, E. W., Gupton, S. L., and Gertler, F. B. (2011) The growth cone cytoskeleton in axon outgrowth and guidance. *Cold Spring Harb. Perspect. Biol.* **3,** p. ii
42. Marx, A., Godinez, W. J., Tsimashchuk, V., Bankhead, P., Rohr, K., and Engel, U. (2013) *Xenopus* cytoplasmic linker-associated protein 1 (XCLASP1) promotes axon elongation and advance of pioneer microtubules. *Mol. Biol. Cell* **24,** 1544–1558
43. Changeux, J. P. (2010) Nicotine addiction and nicotinic receptors: lessons from genetically modified mice. *Nat. Rev. Neurosci.* **11,** 389–401
44. Yevenes, G. E., Peoples, R. W., Tapia, J. C., Parodi, J., Soto, X., Olate, J., and Aguayo, L. G. (2003) Modulation of glycine-activated ion channel function by G protein βγ subunits. *Nat. Neurosci.* **6,** 819–824
45. Nordman, J. C., Muldoon, P., Clark, S., Damaj, M. I., and Kabbani, N. (2014) The α4 nicotinic receptor promotes CD4+ T-cell proliferation and a helper T-cell immune response. *Mol. Pharmacol.* **85,** 50–61
46. Fischer, H., Liu, D. M., Lee, A., Harries, J. C., and Adams, D. J. (2005) Selective modulation of neuronal nicotinic acetylcholine receptor channel subunits by Go-protein subunits. *J. Neurosci.* **25,** 3571–3577
47. Kabbani, N., Woll, M. P., Levenson, R., Lindstrom, J. M., and Changeux, J. P. (2007) Intracellular complexes of the β2 subunit of the nicotinic acetylcholine receptor in brain identified by proteomics. *Proc. Natl. Acad. Sci. U.S.A.* **104,** 20570–20575
48. Kater, S. B., and Mills, L. R. (1991) Regulation of growth cone behavior by calcium. *J. Neurosci.* **11,** 891–899
49. Gomez, T. M., and Zheng, J. Q. (2006) The molecular basis for calcium-dependent axon pathfinding. *Nat. Rev. Neurosci.* **7,** 115–125
50. Nakata, H., and Kozasa, T. (2005) Functional characterization of Gαo signaling through G protein-regulated inducer of neurite outgrowth 1. *Mol. Pharmacol.* **67,** 695–702

Received for publication February 7, 2014.
Accepted for publication March 17, 2014.